URSI GASS 2023, Sapporo, Japan, 19 – 26 August 2023

Commissioning Observations in 2022 with 100-GHz MKID Camera at Nobeyama 45-m Telescope

S. Honda[(1)(2)], M. Nagai[(3)], Y. Murayama[(3)], H. Lee[(4)], Y. Ishizaki[(4)], T. Nitta[(1)(2)], N. Kuno[(1)(2)], H. Matsuo[(3)], Y. Sekimoto[(5)], T. Noguchi[(6)], M. Naruse[(7)], N. Nakai[(8)]
(1) Division of Physics in Faculty of Pure and Applied Sciences, University of Tsukuba,
e-mail: honda.shunsuke.fe@u.tsukuba.ac.jp
(2) Tomonaga Center for the History of the Universe (TCHoU), University of Tsukuba
(3) Advanced Technology Center (ATC), National Astronomical Observatory of Japan (NAOJ)
(4) Degree Programs in Pure and Applied Sciences, Graduate School of Science and Technology, University of Tsukuba
(5) Institute of Space and Astronautical Science (ISAS), Japan Aerospace Exploration Agency (JAXA)
(6) The University of Electro-Communications
(7) Graduate School of Science and Engineering, Saitama University
(8) School of Science and Technology, Kwansei Gakuin University

Abstract

The observations at the 100 GHz frequency band evaluate thermal dust radiations and free-free emission characteristics of star-formation regions in the Milky Way. In our collaboration, the continuum camera with microwave kinetic inductance detector (MKIDs) is being developed for sub-millimeter astronomy. MKID is a resonator-based superconducting detector having an intrinsic potential to get over 1,000 pixels in one readout line. This large number of pixels can realize high sensitivity and wide sky coverage to observe detailed structures of astronomical objects. The camera with 109 MKID pixels for the 100-GHz frequency band was installed at the Nobeyama 45-m telescope in 2021. After the success of MKID performance evaluation with commissioning planet observations, several observations of star-formation regions (W49 and W51) and a quasar of 3C 273 were performed in 2022. This report shows the overview of our instruments installed in the Nobeyama 45-m telescope with their performances and preliminary observational results in 2022.

1 Introduction

Free-free and thermal dust emissions are the main components of millimeter and sub-millimeter continuum radiation from star-forming regions in the Milky Way. They provide crucial information about dust mass and star formation rate. The two emission components are almost equally measured in the 100-GHz frequency band where their SEDs intersect. Therefore, the 100-GHz observations can validate their SED models and constrain their transit frequency. In the 100-GHz band, since the SED is almost minimum, precise SED measurements can also verify whether there are unobserved small contributions such as anomalous microwave emission (AME). AME has been observed with a peak at 10-30 GHz in several HII regions, but the mechanism is not well understood [1]. Precise SED measurements are crucial to determine each component SED in each star-forming region and understand the detailed star formation process in the Milky Way. It is also important in polarization observations of Cosmic Microwave Background (CMB) since modeling of Galactic foreground emissions has significant systematic uncertainties in CMB *B*-mode measurements.

In order to realize the wide observation surveys with a low enough noise level, we are developing a large format camera for millimeter and sub-millimeter wave ranges by utilizing a Microwave kinetic inductance detector (MKID) [2]. MKID is a superconducting sensor with intrinsic frequency multiplexing capability and is adapted to our camera system. MKID consists of a 1/4 wavelength resonator of coplanar waveguide (CPW) geometry. The twin slot antenna tuned for the observation frequency band is connected at the resonator short end, while the CPW feedline is coupled at the open end. Since MKID can stably keep its detector yield due to the relatively simple fabrication process, MKID has been developed as a large-pixel array camera. A silicon lens array with an anti-reflective coating is chosen to be attached to the MKID array in this camera to focus incoming radiation on the antenna. Absorbed energy into the resonator via the antenna changes the properties of the resonator such as a resonant frequency (f_r) and quality factor. The responses of properties are obtained as the forward transmission (S_{21}) of the feedline by using a readout wave of O(GHz).

2 100-GHz MKID Camera and Observations at NRO in 2022

The 109-pixel array of hybrid-type MKIDs [3, 4] with aluminum and NbTiN was adapted to 100-GHz observations, which was fabricated at the Advanced Technology Center (ATC) of NAOJ to improve the sensitivity more than the 2018 first commissioning observation [5]. The optical system was also upgraded by applying anti-reflective structures

This paper's copyright is held by the author(s). It is published in these proceedings and included in any archive such as IEEE Xplore under the license granted by the "Agreement Granting URSI and IEICE Rights Related to Publication of Scholarly Work."

on the vacuum window and silicon lenses to decrease the optical loss [6]. Figure 1 shows the MKID camera receiver for this observation. The receiver uses the combination of dilution (Taiyo Nippon Sanso Co.) and Gifford-McMahon (Sumitomo Heavy Industries, Ltd.) refrigerators [7] to cool down the focal plane. The instrument was installed on the Nobeyama 45-m telescope of Nobeyama Radio Observatory in 2021 [5]. The detector was operated at ~ 85 mK.

Our MKID readout system "FSP" utilizes a frequency sweeping scheme to get time-ordered data (TOD) of resonant frequencies instead of taking TOD of S_{21} with fixed-frequency [8, 9]. This measures frequency sweepings of S_{21} for all MKID resonant frequencies simultaneously every 1/256 seconds, where each frequency point is taken at 10 k sampling-per-second. FSP covers a wide range of responses from the sky temperature of ~ 30 K to ~ 300 K calibration source during the observation. The synchronization between our DAQ system and telescope control has already been established [8] and was operated well in the 2022 observation.

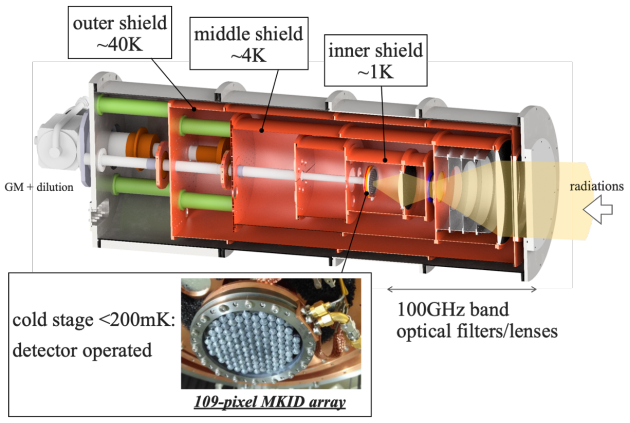

Figure 1. Overview of 100-GHz MKID camera receiver. The lens-coupled 109-pixel MKID array is mounted on the cold stage < 200 mK.

We did MKID performance evaluations with commissioning planet observation datasets in 2021 [5]. Scientific astronomical objects such as star-formation regions (W49 and W51) and one quasar (3C 273) were observed as well as planets in March and April of 2022. In this paper, very preliminary maps of W49 and 3C 273 were reported. The telescope was operated with raster-scan mode to perform the observation of each object where the calibration source at ambient temperature was loaded to the receiver before and after scanning. The center of the scanned region of $4' \times 4'$ in equatorial coordinates was set to the astronomical target position. Beam resolution (full-width-half-maximum) during the observations in 2022 was expected to be $16.7''$.

After the observational data was converted to f_r TODs of 256 Hz by fitting resonance spectra of the MKID array, f_r was calibrated to the antenna temperature T_a^* using a standard chopper wheel method [10]. The created map from T_a^* TOD has a significant temperature gradient along elevation due to different air masses. In order to simply suppress this effect, each scan data in one line was subtracted by T_a^* offset estimated from data during the telescope turns around.

During the commissioning periods, skydip observations have been regularly performed. While the elevation (EL) was changed widely from 18° to 80°, the sky response was modulated by the chopper with the black body radiation of the ambient temperature (referred to as "load"). As shown in Figure 2, the resonant frequency response with relation to the elevation angle is well obtained. When the telescope sees a smaller elevation, higher-temperature radiation is loaded into the array due to higher air mass. Measured resonant frequency ($f_r^{\rm meas}$) can be described as

$$f_r^{\rm meas} = f_r^{\rm load} + \frac{df_r}{dT} T_{\rm atm} \left(1 - e^{-\tau_0 / \sin EL}\right) \qquad (1)$$

where $f_r^{\rm load}$ is the resonant frequency with load condition, $T_{\rm atm}$ is atmospheric temperature, and τ_0 is the atmospheric opacity at the zenith angle. The responsivity of each MKID (df_r/dT) is evaluated using this measurement by fitting data with Equation 1.

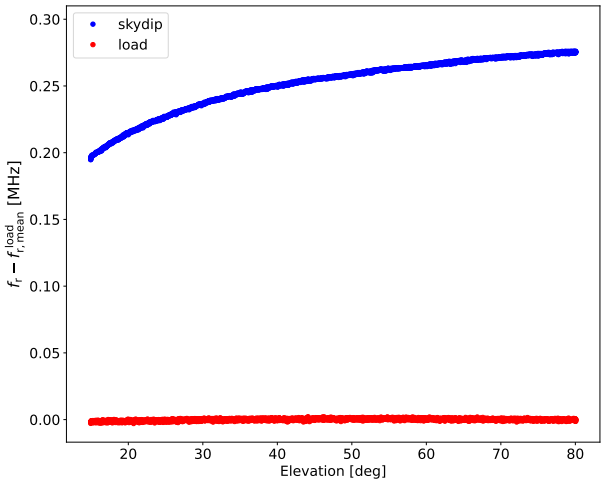

Figure 2. The resonant frequency shift from the average of the load condition as a function of elevation angle. The sky response is chopped every 10 Hz with black body radiation of the ambient temperature. Two components are separately plotted in this figure.

2.1 Star-forming region W49

W49 is a Galactic radio source that can be categorized into two components, thermal component "W49A" and supernova remnant "W49B". W49A is the most luminous star-formation region in the Milky Way ($\sim 10^{7.2} L_\odot$ [11]), embedded in one of the most massive giant molecular clouds ($\sim 10^6 M_\odot$ [12, 13]). Although the extension of molecular clouds is over 100 pc, star formation is concentrated in the central ~ 20 pc. The most prominent region is W49 north (W49N). It is located at $l = 43.1^\circ$, $b = 0.0^\circ$ in the Galactic coordinates with a direct parallax distance from

This paper's copyright is held by the author(s). It is published in these proceedings and included in any archive such as IEEE Xplore under the license granted by the "Agreement Granting URSI and IEICE Rights Related to Publication of Scholarly Work."

Earth, 11.1 kpc [14]. Nearby star formation condensation regions are observed in W49 south (W49S, $\sim 2'$ southeast of W49N) and W49 southwest (W49SW, $\sim 1.5'$ southwest of W49N).

The 33-hour W49A observations in 9 days were performed in March and April 2022 with the 100-GHz MKID camera. In each observation set, only pixels detecting bright W49N signals well are processed. The reconstructed map is shown in Figure 3 by combining 1612 scans. W49N, W49SW, and W49S are well separated.

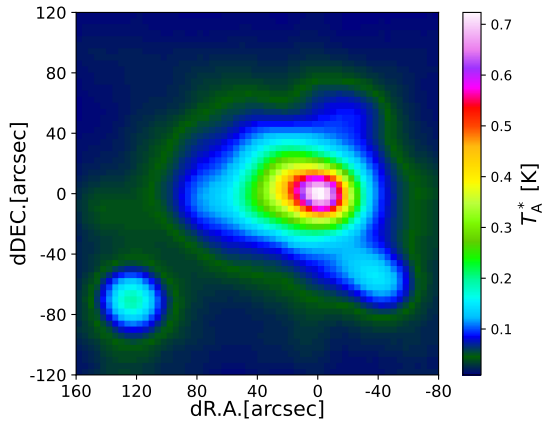

Figure 3. Reconstructed W49A by 100-GHz MKID camera. The largest emission is observed at the W49N cluster. W49S is also seen at a $2.4'$ distance from W49N at the lower left. In the lower right, W49SW is observed as well. The map was smoothed with a Gaussian beam, resulting in the FWHM of the map being $33''$.

2.2 Quasar 3C 273

Quasar 3C 273 is one of the brightest extragalactic objects and the closest quasars [15]. It is observed as the point source with the 100-GHz MKID camera at the 45-m Nobeyama telescope and can be used to evaluate beam characteristics. One observation was performed each day, which resulted in $\sim$ 2-hour observations in 5 days. Figure 4 shows the observed image of 3C 273, where the bright object was detected even with one MKID pixel of one scan-set.

3 Conclusion

In this paper, we reported highlights of observation results with a 100-GHz MKID camera for the Nobeyama 45-m telescope of Nobeyama Radio Observatory in 2022. Due to the sensitivity improvements by NbTiN-Al hybrid MKID newly fabricated in ATC NAOJ and optical system with anti-reflective structures, data for several scientific observations were successfully taken. The maps of star-forming region W49A and quasar 3C 273 were reasonably well reconstructed with low pixel noise levels. The receiver was

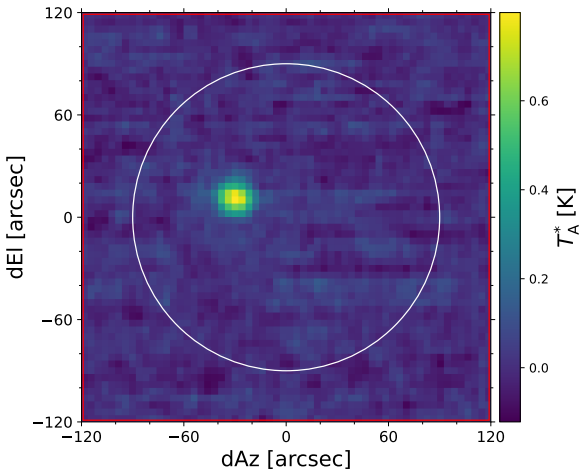

Figure 4. Reconstructed 3C 273 quasar by 100-GHz MKID camera. The large emission of 3C 273 convolved with the beam width can be detected. This map was created by one scan map of one MKID pixel. The radius of the white circle is $90''$ which is the field of view of the MKID camera.

brought back to the laboratory at ATC NAOJ after the observations shown in this paper. After further improving the MKID noise level to achieve the photon-noise-limited condition, scientific observations for various astronomical targets will start.

Acknowledgements

This work was supported by JSPS KAKENHI Grant Number JP26247019. The fabrications and evaluations were realized with ATC NAOJ facilities. We would like to thank the staff at Nobeyama Radio Observatory for their support in installation and operation works. We would like also to thank the people who joined the observation operations, Ayako Niwa, Miwa Aoki, Taichi Kayano, Risa Kurosawa, and Tomohiro Koseki.

References

[1] Planck Collaboration, "Planck intermediate results. XV. A study of anomalous microwave emission in Galactic clouds" *Astronomy and Astrophysics* **565**, A103, 2014.

[2] P. Day et al., "A broadband superconducting detector suitable for use in large arrays." *Nature* **425**, 817–821, 2003.

[3] S. J. C. Yates et al., "Photon noise limited radiation detection with lens-antenna coupled microwave kinetic inductance detectors." *Appl. Phys. Lett.* **99**(7), 073505, 2011.

[4] R. Janssen et al., "High optical efficiency and photon noise limited sensitivity of microwave kinetic inductance detectors using phase readout." *Appl. Phys. Lett.* **103**(20), 203503, 2013.

This paper's copyright is held by the author(s). It is published in these proceedings and included in any archive such as IEEE Xplore under the license granted by the "Agreement Granting URSI and IEICE Rights Related to Publication of Scholarly Work."

[5] S. Honda et al., “Development and Commissioning of 100 GHz MKID Camera at Nobeyama 45m Telescope”, *URSI RSL* submitted, 2022.

[6] T. Nitta et al., “Anti-reflection structures for large-aperture cryogenic lenses and vacuum window in 100-GHz band,” Proc. SPIE 11453, Millimeter, Submillimeter, and Far-Infrared Detectors and Instrumentation for Astronomy X, 114534C, 13, December 2020.

[7] S. Sekiguchi et al., “Development of a Compact Cold Optics for Millimeter and Submillimeter Wave Observations,” *IEEE Transactions on Terahertz Science and Technology*, vol. 5, no. 1, January 2015, pp. 49-56.

[8] M. Nagai et al., “Data Acquisition System of Nobeyama MKID Camera.” *J Low Temp Phys* **193**, 585–592, 2018.

[9] M. Nagai et al., “Resonance Spectra of Coplanar Waveguide MKIDs Obtained Using Frequency Sweeping Scheme.” *J Low Temp Phys* **199**, 250–257, 2020.

[10] T. Wilsonet al., “Tools of Radio Astronomy”, 2013

[11] W. Sievers et al., “Dust emission from star forming regions. I. The W 49A and W 51A complexes.” *Astronomy and Astrophysics*, **251**, p. 231, 1991

[12] R. Simon et al., “The Structure of Four Molecular Cloud Complexes in the BU-FCRAO Milky Way Galactic Ring Survey” *The Astrophysical Journal*, **551**, 2, pp. 747-763, 2001

[13] R. Miyawaki “A Large-Scale ^{13}CO Mapping of the W 49 A Molecular Cloud Complex” *Publications of the Astronomical Society of Japan*, **61**, 1, pp.39–49, 2009

[14] B. Zhang et al., “Parallaxes for W49N and G048.60+0.02: Distant Star Forming Regions in the Perseus Spiral Arm” *The Astrophysical Journal*, **775**, 1, article id. 79, 13 pp., 2013

[15] M. Schmidt, “3C 273 : A Star-Like Object with Large Red-Shift” *Nature*, **197**, 4872, pp. 1040, 1963

This paper’s copyright is held by the author(s). It is published in these proceedings and included in any archive such as IEEE Xplore under the license granted by the “Agreement Granting URSI and IEICE Rights Related to Publication of Scholarly Work.”